Research Article Vol. 30, No. 12 / 6 Jun 2022 / Optics Express 21977
Optics EXPRESS

Highly switchable absorption in a metal hydride device using a near-zero-index substrate

KEVIN J. PALM,[1,2] LISA J. KRAYER,[2,3] AND JEREMY N. MUNDAY[4,*]

[1]Department of Physics, University of Maryland, College Park, MD 20742, USA
[2]Institute for Research in Electronics and Applied Physics, University of Maryland, College Park, MD 20742, USA
[3]Department of Electrical and Computer Engineering, University of Maryland, College Park, MD 20742, USA
[4]Department of Electrical and Computer Engineering, University of California, Davis, CA 95616, USA
[*]jnmunday@ucdavis.edu

Abstract: Optical switchability is an important functionality for photonic devices, which allows them to accommodate a wide range of applications. One way to achieve this switchability is to utilize the reversible and tunable optical changes of metal hydrides. When exposed to H_2 gas, certain metals go through dramatic changes in optical properties as hydrogen atoms expand the lattice spacing. In this paper, we propose a switchable absorption device consisting of a Pd-capped Mg thin film deposited onto a near-zero-index substrate. By utilizing Mg's extreme optical changes upon hydrogenation and combining it with the high optical contrast of the near-zero-index substrate, we can create a device that is fully switchable from a highly reflective state to a broadband absorbing state. When modeling the substrate as a Drude material with a plasma wavelength of 600 nm, we calculate an absorption change of > 70% from 650–1230 nm, with a peak total absorption of 78% at 905 nm. We experimentally demonstrate this effect using 25 nm of Mg with a 3 nm Pd capping layer deposited onto an ITO-coated glass substrate. This device achieves an absorption change of 76% at 1335 nm illumination, with a maximum absorption of 93% in the hydride state, utilizing ITO's near-zero-index region in the near-infrared. By tuning the near-zero-index region of the substrate, this effect can be extended from the visible through the infrared.

1. Introduction

Switchable absorption across the electromagnetic spectrum is a highly desirable functionality for applications from thermography to solar absorbers and color displays. [1–4] Different absorption bandwidths are necessary for these different applications, with solar applications requiring high functionality in the visible, while telecom sensors require the sensitivity to be in the near-infrared. Specifically, absorption in thin metal films has found wide application in hot carrier photodetection and solar cells, where hot carriers created in the metallic thin film can be harnessed. [5–11] By adding a switchable functionality to this effect, devices can be turned on and off with an external stimulus, allowing a wider range of applications, such as switchable solar windows or solar cells. [12,13]

There are multiple ways to achieve switchable absorption for these various applications. One common method is to electrically trigger the optical change, whether by applying a voltage across a diode structure, [14,15] by electronically aligning a liquid crystal array, [16] by actuating a micro-electro-mechanical system, [17] or by electrostatically doping an active optical material, such as graphene. [18] Another method is to thermally activate a phase change in the device, such as with VO_2, which goes through a phase transition at 68°C. [19–22] Alternatively, these optical changes can be triggered by atmospheric changes, such as H_2 gas exposure. Metal hydrides

#450724 https://doi.org/10.1364/OE.450724
Journal © 2022 Received 8 Dec 2021; revised 10 May 2022; accepted 18 May 2022; published 3 Jun 2022

Optics EXPRESS

have recently been utilized for their switchable optical properties in the visible and near-infrared for various purposes including hydrogen sensing and physical encryption. [1,23–30] Mg in particular exhibits a dramatic optical change upon H_2 exposure, transitioning to a dielectric MgH_2. [24,31,32] This change upon hydrogenation can be utilized to switch a device from a highly reflective metallic state to an absorbing state. This effect has been utilized for switchable solar absorption with ~60% absorption change with a Mg-Ti alloy [2] as well as Mg and rare earth-Mg alloys as switchable absorptive mirrors with ~30% absorption change. [33] Many other switchable absorption designs are based on metamaterials that require complex fabrication procedures. In contrast, devices based on thin film Mg only require a thin film deposition and no lithographical processing, although some complexity is added to the switching process due to the necessity of hydrogen gas exposure compared to an electrical pulse.

To further increase the functionality of thin film devices, the optical properties of the substrate can be tuned to create a Fabry-Perot-like resonance within the active layer. [5,34–36] By optimizing the reflection at the thin film/substrate interface, strong destructive interference can be engineered, causing high absorption in the film. For many thin metal films, this effect can be strongly enhanced in the presence of a near-zero-index (NZI) substrate where the real part of the index of refraction approaches zero. Unlike traditional Fabry-Perot resonances that require the thickness of the thin film to be a quarter of the wavelength of the incident light, utilizing this effect allows for interference effects in films 10-100x thinner. Recently, NZI materials have been utilized for a wide range of applications, from light funneling to perfect absorbers, amongst many others. [37–40]

In this manuscript, we propose a thin film device structure for switchable absorption that can be tuned across the visible into the near-infrared spectrum by adjusting the NZI resonance of the substrate, achieving >90% absorption experimentally. The structure consists of a 25 nm Mg layer capped with 3 nm of Pd on an NZI coated glass. By utilizing the extreme optical properties change of Mg upon hydrogenation, we can switch the device from a highly reflective metallic state to a light-absorbing hydride state. Simulations show this effect can create a > 70% change in absorption over a range of 650 -1230 nm when the substrate is modeled as a Drude material with a plasma resonance $\lambda_p = 600$ nm and a damping factor $\gamma = 10^{13}$ Hz, with a peak absorption change of 78% at 905 nm. We experimentally demonstrate this structure on an ITO substrate with an NZI resonance in the near-infrared and find a peak absorption change of 76% at 1335 nm, where the absorption in the hydride state is 93%. This peak absorption change is found to be >15% higher than other metal hydride switchable devices, with similar absorption values in the hydrogenated state. [2]

2. Concept and design

Our switchable absorption structure is depicted in Fig. 1. It consists of a SiO_2 base coated with 350 nm of NZI (labeled substrate), 25 nm Mg, and 3 nm of Pd. The Pd capping layer is necessary for this design to catalyze the H_2 dissociation reaction on the top of the structure. [32,41] The Pd also acts as a protective layer above the Mg, preventing oxidation into MgO. [42,43] Exposure to H_2 gas switches the device from a reflective metallic state into an absorbing hydrogenated state. The H_2 dissociates into H atoms at the Pd surface and diffuses through the thin Pd layer into the Mg to form MgH_2. As Pd hydrogenates into PdH_x, where the hydrogen atoms occupy the interstitial octahedral sites in the metal lattice, it becomes less conductive, but remains in a metallic state. Meanwhile, Mg transforms into a dielectric upon hydrogenation, with the hydride displaying both covalent and ionic bond properties. [44] In this dielectric state, the light is now able to pass through the MgH_2 and interact with the substrate, as opposed to being almost entirely reflected by the Mg layer in the metallic state (see Figure S1 for simulated reflection and transmission plots for each state).

Optics EXPRESS

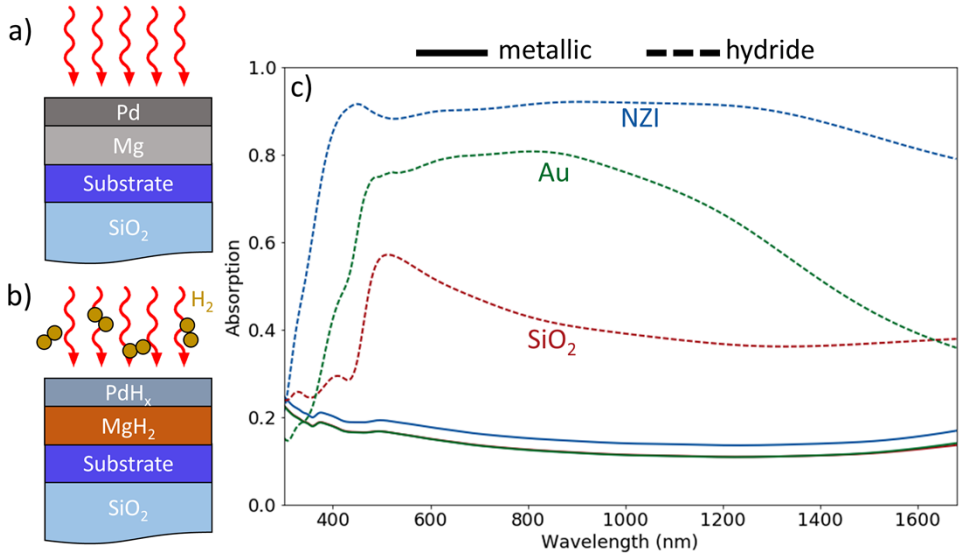

Fig. 1. Device design and simulated absorption spectra for various substrates. a) Device architecture in the inert, metallic state, and b) when exposed to H_2. For each substrate (SiO_2, Au, or NZI), the thicknesses of the Mg and Pd layers were optimized between 3 - 50 nm for maximum absorption change. For the NZI substrate, the thicknesses used were $t_{Pd} = 3$ nm and $t_{Mg} = 25$ nm. For both the Au and SiO_2 substrates, the thicknesses were $t_{Pd} = 3$ nm and $t_{Mg} = 50$ nm. The substrate for each case was kept constant at 350 nm. c) Absorption spectra of the metallic layers (Pd + Mg) with SiO_2 (red), Au (green), and NZI (blue) substrates. The solid (dashed) lines are the spectra in the metallic (hydride) state. The absorption curves for SiO_2 and Au substrates are almost completely overlapping in the metallic state. The NZI substrate is defined to have an index of $\tilde{n} = 0.01 + 1i$ across the spectrum. These simulations account for the 30% volume expansion of Mg upon hydrogenation (e.g. 25 nm metallic Mg becomes 32.5 nm MgH_2).

In Fig. 1(c) we compare our proposed structure to other physical substrates by simulating the absorption spectra using the transfer matrix method found in the literature. [45] Optical properties for the Mg, Pd, and their hydrides are taken from Palm et al., [23] Au from Johnson and Christy, [46] and SiO_2 from Gao et al. [47] The index of the NZI material was defined to be $\tilde{n} = 0.01 + 1i$ (effects of dispersion are discussed and modeled below). In the simulations, the SiO_2 base was considered to be semi-infinite and each substrate was defined to be 350 nm. For the Au substrate, 350 nm is optically thick, so that the device can be practically thought of as an infinite Au substrate, and because the SiO_2 substrate layer is on a SiO_2 base, the defined thickness does not affect the results as the substrate is continuous with the base layer. For the NZI material, we find that as the substrate thickness increases, we achieve a greater absorption change in the material. Once the substrate becomes greater than ~300 nm, this effect begins to level off. We chose 350 nm to achieve this high absorption change, while still having a thin enough layer that is reasonably achieved in common NZI materials, such as transparent conducting oxides (TCO). [48,49] For the complete spectral dependence of the NZI substrate thickness on the absorption change, see Figure S2.

For each different substrate, we optimized the Mg and Pd thicknesses that would create the largest absorption change upon hydrogenation. We define the total absorption as the combined absorptions in the Pd and Mg layers (note: absorption in the substrate and SiO_2 are negligible, see for example Figure S4). In our thickness optimization, we applied the maximum thickness of

Optics EXPRESS

Mg as 50 nm. The full Mg film would not hydrogenate if it were greater than 50 nm due to the formation of a well-documented MgH_2 hydrogen blocking layer. [31,50] We applied a lower thickness bound of 3 nm on the Pd layer to ensure a uniform film and complete coverage of the Mg. Expansion of the metal hydrides also needs to be taken into account, as the lattice expands as hydrogen enters the material. The Mg lattice is found to expand by 30% upon hydrogenation [31] (e.g. 25 nm metallic Mg becomes 32.5 nm MgH_2), and this effect was included in all simulations. Pd has a much smaller lattice expansion, about 12%, [51] which ended up being negligible in our simulations since the optimized Pd thicknesses were very small. We found the optimized thicknesses for each layer were $t_{Pd} = 3$ nm and $t_{Mg} = 25$ nm for the NZI substrate and $t_{Pd} = 3$ nm and $t_{Mg} = 50$ nm for both the Au and SiO_2 substrates. See Figure S3 for contour plots of the absorption change as a function of the Mg and Pd thicknesses at different wavelengths.

In the metallic state, Mg is optically opaque at a thickness of 50 nm, so the absorption curves for the device stacks with SiO_2 and Au substrates in Fig. 1(c) almost entirely overlap. In the NZI material case, the light slightly transmits through the Mg layer at a thickness of 25 nm but is still mostly reflected with little measured absorption, under 20% for most of the spectrum. Upon hydrogenation, we see a dramatic increase in absorption for each substrate. The extremely reflective Mg becomes a partially transmitting MgH_2. We see that the choice of substrate greatly affects the absorption in the metal hydrides, as the light now interacts at the MgH_2/substrate interface. For the SiO_2 substrate, we see the smallest increase in absorption, mostly due to the increase in path length of the light in the metal hydrides as the light transmits through it, with little added benefit from the reflection off the substrate interface. The Au substrate shows a much higher absorption increase by creating a cavity effect within the MgH_2, with light reflecting between the Au substrate and PdH_x capping layer. The largest attainable absorption change is found for the NZI substrate. In this case, a strong Fabry-Perot-like cavity is created within the MgH_2, creating high absorption due to the destructive interference effects. With these defined optical properties, we can achieve an absorption of >80% from 400–1650 nm and >90% from 625–1300 nm in the hydride state. We note that the large broadband result depicted by the NZI substrate in Fig. 1(c) is not possible with a realistic substrate, because a constant complex index of refraction over this entire wavelength region does not obey Kramers-Kronig consistency. Instead, this result shows the potential for this high switchable absorption response across the visible spectrum and into the infrared if the substrate's index of refraction has a low real part with the imaginary part close to 1 for any span of these wavelengths. We also note that there will be some alloying between the Pd and Mg layers upon deposition. [32] To avoid this alloying in thin film stacks, it is common to use a Ti interlayer between the Mg and Pd layers. The optical properties being used for these simulations were taken on a thin film stack without this Ti interfacial layer, thus the properties being used are accurate for these simulations and account for this interfacial layer.

The absorption of the light in the hydride layers is split between the PdH_x and MgH_2. The PdH_x layer is responsible for the majority of the short-wavelength absorption up to ~500 nm. At this point, the MgH_2 begins to absorb more light, with the absorption in the Pd tapering off. The reason for this delineation is that PdH_x still behaves optically like a metal with higher attenuation for shorter wavelengths. It gets a large increase in absorption from the cavity effect, with the path length of light traveling through it increasing dramatically from the multiple reflections within the MgH_2. The MgH_2 has higher attenuation beginning in the upper visible region, which is where it begins to dominate the absorption. The combination of the absorption in these two layers allows for the near-constant absorption change observed in Fig. 1(C). To see the full breakdown of absorption between each layer in the stack, see Figure S4.

Having found this strong absorption effect for the structure with a tailored index of refraction $\tilde{n} = 0.01 + 1i$, we now explore in-depth how the optical properties of this substrate layer affect the total absorption change in the metal films and how robust this effect is. Figure 2 shows the

Optics EXPRESS

relationship of the complex index of refraction of the substrate, $\tilde{n} = n + ik$, with the change in absorption of the metal films. Δ Absorption is defined as the absorption of the metal layers (Pd and Mg) subtracted from the absorption in the metal hydrides after H_2 exposure (PdH_x and MgH_2). The first trend that is evident with these plots is that the absorption change increases with decreasing n for each wavelength, showing the necessity of using an NZI substrate. A more interesting trend occurs with the imaginary part of the index. Upon first consideration, we would expect that the absorption in the metal hydrides would be maximized with a maximum reflectivity at the MgH_2/substrate interface. We find through our simulations that this is not the case, because the reflectivity R is maximized when $k = 0$ for the substrate for all investigated wavelengths (see Figure S5) and that the absorption is maximized for $k \approx 1$ for incident wavelengths $\lambda = 800$, 1200, and 1600 nm and $k \approx 2$ for $\lambda = 400$ nm. This analysis shows that the absorption increase in the metals is not solely from an increased path length from a perfect reflection off the NZI substrate, but from creating an additive destructive interference condition within the metals. For short wavelengths (e.g. 400 nm) and fixed n, the absorption strongly depends on k and increases for larger k (Fig. 2(a)). However, for longer wavelengths (800, 1200, and 1600 nm), the absorption is nearly independent of k when $n > 0$ .25 (Fig. 2(b), 2(c), 2(d). When $n < 0.25$, we observe a more pronounced dependence on k, as outlined above. For the pure absorption plots for the metallic and hydride states (plots subtracted to give the change in absorption), see Figures S6 and S7.

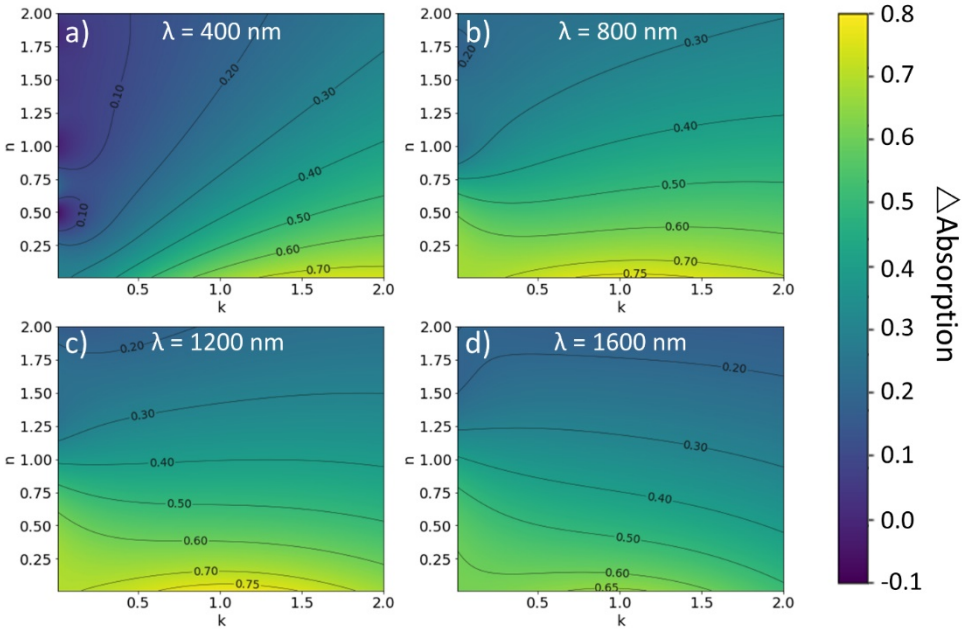

Fig. 2. Effect of the NZI layer's optical properties, $\tilde{n} = n + ik$, on full stack absorption change. Device stack is defined as a SiO_2 substate, 350 nm of NZI material (whose properties we are investigating), 25 nm of Mg, and capped with 3 nm Pd. Absorption change is defined as the absorption of the device in the metallic state subtracted from the absorption in the hydrogenated state. λ represents different incident wavelengths of illumination, here showing a) $\lambda = 400$ nm, b) $\lambda = 800$ nm, c) $\lambda = 1200$ nm, d) $\lambda = 1600$ nm.

So far our consideration for this structure has used specifically chosen refractive indices, but a real material has to obey causality across the spectrum. To apply a model that obeys

Optics EXPRESS

Kramers-Kronig consistency, we modeled our substrate as a Drude material with properties:

$$\tilde{n} = \sqrt{\epsilon(\omega)} = \sqrt{\epsilon_\infty - \frac{\omega_p^2}{-\omega^2 + i\,\gamma\,\omega}}$$

where $\tilde{n}$ is the complex index of refraction, ε is the dielectric function, ε_∞ is the permittivity as $\omega \rightarrow \infty$, ω_p is the plasma frequency, and γ is the damping constant. This equation models the free-electron response of a metal without any interband transitions but provides for a realistic, yet simple, model of an NZI material.

Figure 3 shows the results of modeling the properties of the substrate layer with a Drude model. For these simulations, we have set ε_∞ to 1 (for effects of ε_∞ on the absorption change, see Figures S8 and S9). We immediately see that with this physical model, we can still achieve very high absorption changes, >75% for some incident wavelengths. The absorption is maximized for smaller γ, although this effect begins to plateau for $\gamma < 10^{14}$ Hz. This effect is what we would expect, as a higher damping term in the substrate causes an increased real part to the index of refraction. The increased damping eliminates the cavity effect in the MgH_2 exploited by the device structure. The $\gamma < 10^{14}$ Hz range is easily achievable, as many TCOs have been found to have a damping coefficient between 10^{13} and 10^{14} Hz. [52] For further details of the damping term versus illumination wavelength over an extended bandwidth, see Figure S10.

The Drude simulations also show a very strong dependence on the plasma wavelength $\lambda_p = 2\pi c/\omega_p$ where c is the speed of light. The resonance effect occurs for plasma wavelengths slightly lower than the illumination wavelength. This occurs because, as we saw in Fig. 2, the absorption effect is maximized for $k \approx 1$ for long wavelength visible and near infrared illumination. In the Drude model, k increases for wavelengths below the plasma frequency, and the effect is greatest when k is large enough to create the phase matching in the MgH_2 and n remains low enough to harness the increased reflection from a near-zero index. For 400 nm illumination, we can achieve >70% absorption change for a Drude material with $\lambda_p \approx 150$ nm and $\gamma < 3*10^{14}$ Hz. A real material that could fulfill these values would be Pt with $\lambda_p = 144$ nm and $\gamma = 1.088*10^{13}$ Hz. [53] For longer wavelengths in the spectrum, we see the continued potential for strong effects, with regions > 75% absorption change for $\lambda = 800$ nm and $\lambda = 1200$ nm. As we continue into the infrared, we find that the high absorption change effect begins to taper off. For the full effect of the plasma wavelength versus illumination wavelength, see Figure S11.

In Fig. 3(e), we find that even when using a Drude model for the NZI material, we still can get a broadband result. In these simulations, we defined $\gamma = 10^{13}$ Hz. For λ_p in the long-wavelength portion of the visible regime, we can see the bandwidth of the response is the greatest. We find that for $\lambda_p = 600$ nm and $\lambda_p = 800$ nm, we can achieve a region of > 70% absorption change for over a 580 nm range (650–1230 nm for $\lambda_p = 600$ nm and 825–1405 nm for $\lambda_p = 800$ nm). If we lower our absorption change threshold to 60%, then our bandwidth widens to 835 nm. Both of these cases reach a peak absorption change of 78%, at 905 nm for $\lambda_p = 600$ nm and at 1145 nm for $\lambda_p = 800$ nm. If we further increase λ_p, we still see a broadband result, but the magnitude of the peak of the absorption change begins to decrease. Conversely, if we lower λ_p, we can still achieve a high peak absorption switchability, but begin to lose the large broadband effect as the resonance narrows.

To test the robustness of this effect to non-normal incidence illumination, we simulated the same structures depicted in Fig. 1 for illumination angles varying from 0°-85°, with the angle θ being defined from the normal. Figure 4 shows the dependence of the absorption in the hydride state on the incident angle. We immediately notice that the NZI substrate remains the best choice for maximum absorption at non-normal angles when compared to the Au and SiO_2 substrates. The only exception to this is at very high incident angles, where for TM polarization the Au substrate begins to either match or slightly outperform the NZI material. In all other cases, the NZI remains strongly superior.

Optics EXPRESS

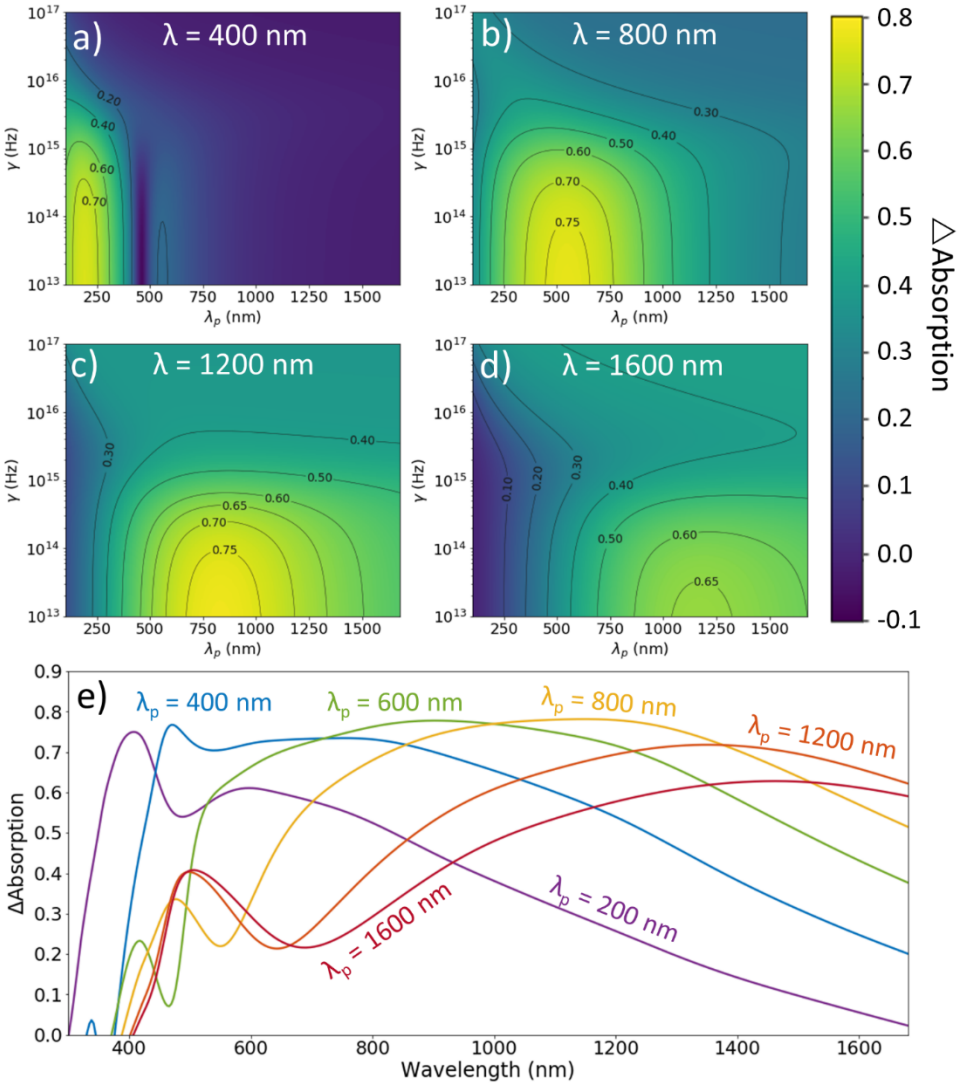

Fig. 3. Change in absorption upon hydrogenation using a Drude model for the NZI material. Device stack is defined as a SiO_2 substate, 350 nm of NZI material (whose properties we are defining with the Drude model), 25 nm of Mg, and capped with 3 nm Pd. λ_p is the plasma wavelength ($\lambda_p = 2\pi c/\omega_p$) and γ the damping term in the Drude model. λ represents different incident illumination wavelengths with a) $\lambda = 400$ nm, b) $\lambda = 800$ nm, c) $\lambda = 1200$ nm, d) $\lambda = 1600$ nm. e) Absorption change vs illumination wavelength for 6 different λ_p with $\gamma = 10^{13}$ Hz, showing how broadband the switchable effect can be.

Optics EXPRESS

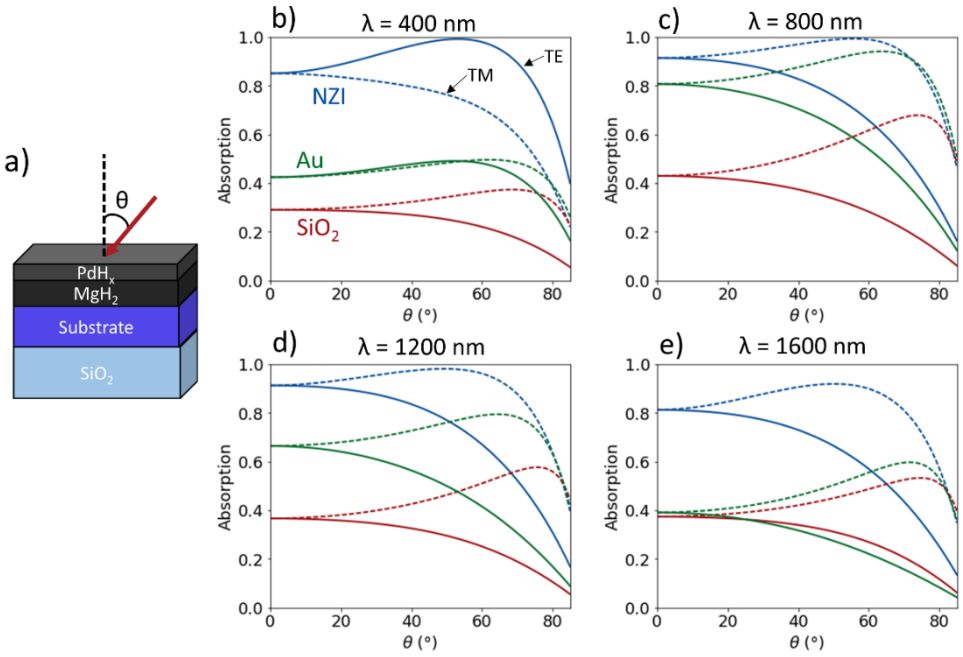

Fig. 4. Angular dependence of incident light on absorption in the hydride state. a) Diagram of the device. θ defined as angle incident light makes with the normal. NZI substrate layer defined to be 350 nm with $\tilde{n} = 0.01 + 1i$, followed by 25 nm of Mg and 3 nm of Pd. b-e) Plots showing the absorption of the structure with increasing θ for four different incident wavelengths b) 400 nm, c) 800 nm, d) 1200 nm, e) 1600 nm. Blue lines represent NZI substrates, green lines represent Au substrates, and red lines represent SiO_2 substrates. Solid (dashed) lines are TE (TM) illumination.

We find that with these increasing angles, the absorption in the hydride state can reach almost perfect absorption. For TE illumination at 400 nm, the hydride absorption reaches 99.2% at 53°. For TM illumination at 800 nm and 1200 nm, the hydride absorption peaks at 99.3% at 56° and 98.1% at 49° respectively. These perfect absorption effects begin to trail off as we continue further into the infrared. This greatly outperforms similar peaks found with the other substrates. The 400 nm behaves differently than the other wavelengths shown here because for this wavelength, the absorption mainly occurs in the PdH_x as opposed to the MgH_2. This difference causes different conditions for the destructive interference in the device, causing very different responses to different polarizations.

The absorption changes also follow similar trends to the absorption in the hydride state. With the exception of 400 nm illumination, we find that the absorption change stays fairly robust (constant) for TM polarization from 0° incident angle all the way to 60° (for 800 nm and 1200 nm illumination the absorption change remains above 70% in this entire region). For TE polarization at 400 nm illumination, we see a dramatic increase in the absorption change with a peak of $\Delta Abs = 88\%$ at 59°. The plots of dependence of absorption change with angle are shown in Figure S13.

3. Experimental demonstration

To demonstrate this effect in practice, we used a film of ITO deposited on a soda-lime glass substrate as our NZI substrate (MSE Supplies). The optical properties of the ITO were measured with spectroscopic ellipsometry (J.A. Woollam M-2000) and fit with a Drude-Lorentz model. See

Optics EXPRESS

Figure S14 for ITO optical properties. The Pd/Mg metal stack was deposited using electron-beam evaporation with a vacuum pressure of $< 4*10^{-4}$ Pa (Denton Vacuum). 25 nm of Mg was deposited at a rate of 5 Å/s followed by a 3 nm Pd cap at 1 Å/s without breaking chamber vacuum. For each deposition, fresh Mg pellets were used to avoid oxide contamination. Immediately after deposition, we measured the transmission and reflection intensities of the device using the ellipsometer. Reflection measurements were taken at 20° incident angle and transmission measurements were taken with normal illumination. Using a custom-designed environmental chamber, we then exposed the device to 1 bar of H_2 gas while dynamically measuring the transmission intensity. The hydrogen gas was input into the chamber at 20 sccm with controlled flow with a mass flow controller (Bronkhorst USA). Gas modelling shows that the chamber reaches 95% H_2 partial pressure after ~15 min. Once the sample had completely loaded, determined by the stabilization of the transmission intensity, we removed the sample from the transmission chamber and measured the reflection intensity. After this measurement, we remeasured the transmission intensity. This intensity spectrum exactly matched that of the in-situ measurement, showing that the sample had not had any appreciable unloading of hydrogen during the brief time outside of the environmental chamber. We repeated this process with the Pd/Mg deposited on a plain glass slide as a control sample.

The experimental absorption changes are shown in Fig. 5 and are in good agreement with simulations. Absorption changes are calculated by using $A = 1\text{-}R\text{-}T$, where A is the absorption, R the reflection intensity, and T the transmission intensity. In this formula, scattering is disregarded. This is a reasonable assumption in our experiments because the RMS roughness of our samples is < 3 nm, thus there will be negligible scattering off the surface. See Figure S15 for topographic AFM measurements of the surface roughness before and after sample hydrogenation. We compare this experimental data to transfer matrix method simulations and see strong agreement for both the ITO and glass substrates. The simulated data uses an incident angle of 20° to match the angle the reflection intensity data was taken. The experimental transmission intensity measurements were taken with normal illumination, but the difference in simulated transmission intensity of

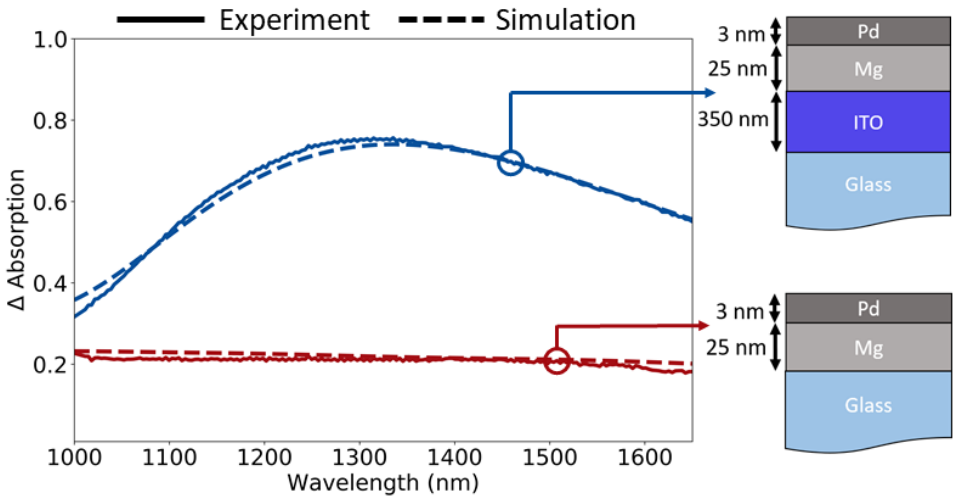

Fig. 5. Experimental demonstration of device performance. Solid lines are experimental data, while dashed lines are simulation data. Blue lines represent the device on an ITO substrate (Top Right), while red lines are on a plain glass substrate (Bottom Right). The experimental data shows good agreement with that expected from simulations. The ITO device reaches a max absorption change of 76% at 1335 nm illumination, while the plain glass device never has an absorption change higher than 21%.

Optics EXPRESS

this device between normal and 20° illumination is < 2% over the reported wavelength range, so we can assume that this difference is negligible on the scale of the effect shown. Figure S16 shows this simulated transmission difference between these two angles.

The ITO device resonance is maximized in the near-infrared at 1335 nm, near ITO's NZI resonance at 1250 nm. The device resonance is red-shifted from the NZI resonance as expected from the simulations because of the necessity of a higher imaginary part of the index for the full absorption effect. The maximum experimental absorption change was found to be 76%, with a maximum total absorption in the hydrogenated state of 93%. This slightly outperforms the simulated maxima of 74% and 87% respectively. Reasons for this discrepancy can be attributed to the slight differences in the optical properties of thin films when deposited on different substrates due to either different grain sizes or surface roughness. The effect is relatively broadband, with an absorption change > 60% from 1140 nm to 1595 nm for a bandwidth of 455 nm for these criteria. The time of loading of the sample, as determined from the dynamic transmission intensity data, was found to be ~30 min (see Figure S17). Figure S18 shows the simulated layer-by-layer absorption in this experimental device stack. Unlike the ideal NZI case, we find that real ITO does have some contribution to the absorption in the device stack, exhibiting a ~8% absorption across the wavelength region shown in Fig. 5. This contribution is still quite small when compared to the combined 77% simulated combined absorption in the PdH_x and MgH_2 layers. This experimental demonstration shows the promise of this device architecture with relative ease of fabrication.

As expected, when the metal stack is deposited on a plain glass substrate, there are no resonance effects, because the glass does not have an NZI region. There is still an absorption change in the material due to the hydrogenation of the Pd/Mg stack, but experimentally we find that it is fairly small and constant across the near-infrared at 21%. See Figure S19 for the individual absorption data for the metallic and hydride states for both the ITO and glass devices.

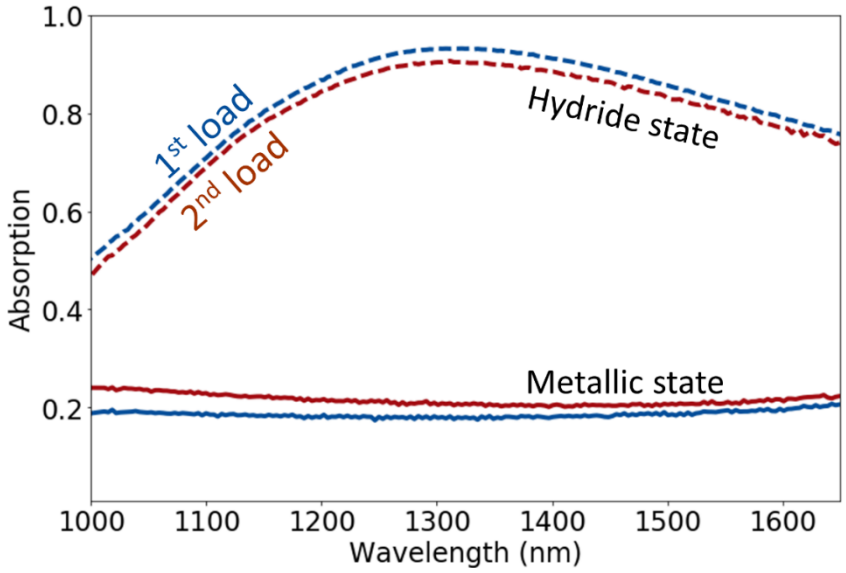

Fig. 6. Reversibility of the ITO switchable absorption device. Solid lines are the device in the metallic state and dashed lines represent the device in the hydride state. The blue lines are the data from the original load, while the red lines indicated the second load. The data shows that the absorption change is reversible, but with a slight decrease in the magnitude of the effect on the second cycle.

Optics EXPRESS

Lastly, we demonstrate the reversibility of this device. To unload the MgH_2, we place the device on a hot plate at 85°C in the ambient atmosphere for 30 min. During this unloading, the device visibly turns back into a metallic state. After the unload, we retake the optical measurements and repeat the loading procedure outlined above. Figure 6 shows the results of this second cycle compared to the original loading. We can see that the effect is mostly reversible on the second cycle, but that the magnitude of the effect is slightly diminished. The metallic state after the unload has slightly higher absorption than the pristine metallic state, which can be attributed to dislocations formed in the Mg lattice upon the original loading. [54,55] The second loaded state still reaches a high total absorption of 91%, compared to 93% on the initial run, demonstrating that the process is reversible.

4. Summary

In summary, we have proposed and experimentally demonstrated a thin film stack of Pd/Mg can achieve switchable high absorption changes by exposure to H_2 gas. By utilizing ITO's NZI resonance in the near-infrared, our device achieves a maximum absorption change of 76%, with a maximum total absorption of 93% at 1335 nm illumination. This device has an absorbing change $> 60\%$ over a 455 nm bandwidth. This is a significant improvement when compared to a control sample consisting of a plain glass slide without the ITO layer, which only achieves an absorption change of 21% over this spectral region. We show that this process is reversible, with only a slight deprecation in total absorption change upon a second cycle.

Our simulations varying the optical properties of the substrate show the potential of expanding this device to other wavelength regimes by using materials with NZI resonances in those frequency bands. We showed that this effect can create a $> 70\%$ change in absorption over a range of 650 -1230 nm incident wavelengths when being modeled as a Drude material with a plasma resonance $\lambda_p = 600$ nm and damping $\gamma < 10^{14}$ Hz, showing that this effect has the potential to be very broadband. This work shows the potential for switchable high absorption devices across different wavelength regions that exploit the NZI behavior of the substrate without affecting other aspects of the device design. Future work will involve investigating new substrates in these different spectral regions, as well as the potential of alloying Mg with other metals to retain this high absorption change while speeding up the dynamics and cyclability of the loading/unloading cycles.

Funding. University of Maryland (Ann G. Wylie Dissertation Fellowship); National Science Foundation (DGE 1322106, ECCS-1554503); National Defense Science and Engineering Graduate; Google.

Acknowledgments. The authors are grateful for fabrication support from the FabLab at the University of Maryland Nanocenter.

Disclosures. The authors declare no conflicts of interest.

Data availability. Data underlying the results presented in this paper are not publicly available at this time but may be obtained from the authors upon reasonable request.

Supplemental document. See Supplement 1 for supporting content.

References

1. X. Duan, S. Kamin, and N. Liu, "Dynamic plasmonic colour display," Nat. Commun. **8**(1), 14606 (2017).
2. A. Baldi, D. M. Borsa, H. Schreuders, J. H. Rector, T. Atmakidis, M. Bakker, H. A. Zondag, W. G. J. van Helden, B. Dam, and R. Griessen, "Mg–Ti–H thin films as switchable solar absorbers," Int. J. Hydrogen Energy **33**(12), 3188–3192 (2008).
3. A. Tittl, A.-K. U. Michel, M. Schäferling, X. Yin, B. Gholipour, L. Cui, M. Wuttig, T. Taubner, F. Neubrech, and H. Giessen, "A Switchable Mid-Infrared Plasmonic Perfect Absorber with Multispectral Thermal Imaging Capability," Adv. Mater. **27**(31), 4597–4603 (2015).
4. S. Daqiqeh Rezaei, Z. Dong, J. Y. En Chan, J. Trisno, R. J. H. Ng, Q. Ruan, C.-W. Qiu, N. A. Mortensen, and J. K. W. Yang, "Nanophotonic Structural Colors," ACS Photonics **8**(1), 18–33 (2021).
5. L. J. Krayer, E. M. Tennyson, M. S. Leite, and J. N. Munday, "Near-IR Imaging Based on Hot Carrier Generation in Nanometer-Scale Optical Coatings," ACS Photonics **5**(2), 306–311 (2018).

Optics EXPRESS

6. C. Hägglund, S. P. Apell, and B. Kasemo, "Maximized Optical Absorption in Ultrathin Films and Its Application to Plasmon-Based Two-Dimensional Photovoltaics," Nano Lett. **10**(8), 3135–3141 (2010).
7. N. Ahmad, J. Stokes, N. A. Fox, M. Teng, and M. J. Cryan, "Ultra-thin metal films for enhanced solar absorption," Nano Energy **1**(6), 777–782 (2012).
8. M. L. Brongersma, N. J. Halas, and P. Nordlander, "Plasmon-induced hot carrier science and technology," Nat. Nanotechnol. **10**(1), 25–34 (2015).
9. T. Gong and J. N. Munday, "Materials for hot carrier plasmonics [Invited]," Opt. Mater. Express **5**(11), 2501–2512 (2015).
10. T. Gong and J. N. Munday, "Angle-Independent Hot Carrier Generation and Collection Using Transparent Conducting Oxides," Nano Lett. **15**(1), 147–152 (2015).
11. T. Gong and J. N. Munday, "Aluminum-based hot carrier plasmonics," Appl. Phys. Lett. **110**(2), 021117 (2017).
12. M. Götz, M. Lengert, N. Osterthun, K. Gehrke, M. Vehse, and C. Agert, "Switchable Photocurrent Generation in an Ultrathin Resonant Cavity Solar Cell," ACS Photonics **7**(4), 1022–1029 (2020).
13. J. Murray, D. Ma, and J. N. Munday, "Electrically Controllable Light Trapping for Self-Powered Switchable Solar Windows," ACS Photonics **4**(1), 1–7 (2017).
14. B. Zhu, Y. Feng, J. Zhao, C. Huang, and T. Jiang, "Switchable metamaterial reflector/absorber for different polarized electromagnetic waves," Appl. Phys. Lett. **97**(5), 051906 (2010).
15. D. Lee, H. Jeong, and S. Lim, "Electronically Switchable Broadband Metamaterial Absorber," Sci. Rep. **7**(1), 4891 (2017).
16. D. Shrekenhamer, W.-C. Chen, and W. J. Padilla, "Liquid Crystal Tunable Metamaterial Absorber," Phys. Rev. Lett. **110**(17), 177403 (2013).
17. P. Pitchappa, C. Pei Ho, P. Kropelnicki, N. Singh, D.-L. Kwong, and C. Lee, "Micro-electro-mechanically switchable near infrared complementary metamaterial absorber," Appl. Phys. Lett. **104**(20), 201114 (2014).
18. S. Thongrattanasiri, F. H. L. Koppens, and F. J. García de Abajo, "Complete Optical Absorption in Periodically Patterned Graphene," Phys. Rev. Lett. **108**(4), 047401 (2012).
19. M. A. Kats, R. Blanchard, P. Genevet, Z. Yang, M. M. Qazilbash, D. N. Basov, S. Ramanathan, and F. Capasso, "Thermal tuning of mid-infrared plasmonic antenna arrays using a phase change material," Opt. Lett. **38**(3), 368–370 (2013).
20. H. Wang, Y. Yang, and L. Wang, "Switchable wavelength-selective and diffuse metamaterial absorber/emitter with a phase transition spacer layer," Appl. Phys. Lett. **105**(7), 071907 (2014).
21. Y. Zhao, Q. Huang, H. Cai, X. Lin, and Y. Lu, "A broadband and switchable VO2-based perfect absorber at the THz frequency," Opt. Commun. **426**, 443–449 (2018).
22. T. Wang, Y. Zhang, Y. Zhang, H. Zhang, M. Cao, and M. Cao, "Dual-controlled switchable broadband terahertz absorber based on a graphene-vanadium dioxide metamaterial," Opt. Mater. Express **10**(2), 369–386 (2020).
23. K. J. Palm, J. B. Murray, T. C. Narayan, and J. N. Munday, "Dynamic Optical Properties of Metal Hydrides," ACS Photonics **5**(11), 4677–4686 (2018).
24. K. J. Palm, J. B. Murray, J. P. McClure, M. S. Leite, and J. N. Munday, "In Situ Optical and Stress Characterization of Alloyed PdxAu1–x Hydrides," ACS Appl. Mater. Interfaces **11**(48), 45057–45067 (2019).
25. S. Bagheri, N. Strohfeldt, M. Ubl, A. Berrier, M. Merker, G. Richter, M. Siegel, and H. Giessen, "Niobium as Alternative Material for Refractory and Active Plasmonics," ACS Photonics **5**(8), 3298–3304 (2018).
26. F. A. A. Nugroho, I. Darmadi, L. Cusinato, A. Susarrey-Arce, H. Schreuders, L. J. Bannenberg, A. B. d. S. Fanta, S. Kadkhodazadeh, J. B. Wagner, T. J. Antosiewicz, A. Hellman, V. P. Zhdanov, B. Dam, and C. Langhammer, "Metal–polymer hybrid nanomaterials for plasmonic ultrafast hydrogen detection," Nat. Mater. **18**(5), 489–495 (2019).
27. R. M. Penner, "A Nose for Hydrogen Gas: Fast, Sensitive H2 Sensors Using Electrodeposited Nanomaterials," Acc. Chem. Res. **50**(8), 1902–1910 (2017).
28. A. Tittl, P. Mai, R. Taubert, D. Dregely, N. Liu, and H. Giessen, "Palladium-Based Plasmonic Perfect Absorber in the Visible Wavelength Range and Its Application to Hydrogen Sensing," Nano Lett. **11**(10), 4366–4369 (2011).
29. Y. Nishijima, Y. Nishijima, T. Kurotsu, N. Yamasaku, H. Takahashii, K. Kurihara, T. Beni, S. Okazaki, T. Arakawa, A. Balčytis, G. Seniutinas, S. Juodkazis, S. Juodkazis, and S. Juodkazis, "Improvement and stabilization of optical hydrogen sensing ability of Au-Pd alloys," Opt. Express **28**(17), 25383–25391 (2020).
30. Y. Nishijima, S. Shimizu, K. Kurihara, Y. Hashimoto, H. Takahashi, A. Balčytis, G. Seniutinas, S. Okazaki, J. Juodkazytė, T. Iwasa, T. Taketsugu, Y. Tominaga, and S. Juodkazis, "Optical readout of hydrogen storage in films of Au and Pd," Opt. Express **25**(20), 24081–24092 (2017).
31. J. Karst, F. Sterl, H. Linnenbank, T. Weiss, M. Hentschel, and H. Giessen, "Watching in situ the hydrogen diffusion dynamics in magnesium on the nanoscale," Sci. Adv. **6**(19), eaaz0566 (2020).
32. A. Baldi, L. Mooij, V. Palmisano, H. Schreuders, G. Krishnan, B. J. Kooi, B. Dam, and R. Griessen, "Elastic versus Alloying Effects in Mg-Based Hydride Films," Phys. Rev. Lett. **121**(25), 255503 (2018).
33. I. A. M. E. Giebels, J. Isidorsson, and R. Griessen, "Highly absorbing black Mg and rare-earth-Mg switchable mirrors," Phys. Rev. B **69**(20), 205111 (2004).
34. M. A. Kats, R. Blanchard, P. Genevet, and F. Capasso, "Nanometre optical coatings based on strong interference effects in highly absorbing media," Nat. Mater. **12**(1), 20–24 (2013).

Optics EXPRESS

35. L. J. Krayer, J. Kim, and J. N. Munday, "Near-perfect absorption throughout the visible using ultra-thin metal films on index-near-zero substrates [Invited]," Opt. Mater. Express **9**(1), 330–338 (2019).
36. C. Hilsum, "Infrared Absorption of Thin Metal Films," J. Opt. Soc. Am. **44**(3), 188–191 (1954).
37. D. C. Adams, S. Inampudi, T. Ribaudo, D. Slocum, S. Vangala, N. A. Kuhta, W. D. Goodhue, V. A. Podolskiy, and D. Wasserman, "Funneling Light through a Subwavelength Aperture with Epsilon-Near-Zero Materials," Phys. Rev. Lett. **107**(13), 133901 (2011).
38. J. Rensberg, Y. Zhou, S. Richter, C. Wan, S. Zhang, P. Schöppe, R. Schmidt-Grund, S. Ramanathan, F. Capasso, M. A. Kats, and C. Ronning, "Epsilon-Near-Zero Substrate Engineering for Ultrathin-Film Perfect Absorbers," Phys. Rev. Appl. **8**(1), 014009 (2017).
39. S. Feng and K. Halterman, "Coherent perfect absorption in epsilon-near-zero metamaterials," Phys. Rev. B **86**(16), 165103 (2012).
40. B. Edwards, A. Alù, M. G. Silveirinha, and N. Engheta, "Reflectionless sharp bends and corners in waveguides using epsilon-near-zero effects," J. Appl. Phys. **105**(4), 044905 (2009).
41. M. A. Pick, J. W. Davenport, M. Strongin, and G. J. Dienes, "Enhancement of Hydrogen Uptake Rates for Nb and Ta by Thin Surface Overlayers," Phys. Rev. Lett. **43**(4), 286–289 (1979).
42. A. M. Vredenberg, E. M. B. Heller, and D. O. Boerma, "Hydriding characteristics of FeTi/Pd films," J. Alloys Compd. **400**(1-2), 188–193 (2005).
43. P. Hjort, A. Krozer, and B. Kasemo, "Hydrogen sorption kinetics in partly oxidized Mg films," J. Alloys Compd. **237**(1-2), 74–80 (1996).
44. G. G. Libowitz, "Metallic hydrides; fundamental properties and applications," J. Phys. Chem. Solids **55**(12), 1461–1470 (1994).
45. M. Born and E. Wolf, *Principles of Optics*, 7th ed. (Cambridge University, 2005).
46. P. B. Johnson and R. W. Christy, "Optical Constants of the Noble Metals," Phys. Rev. B **6**(12), 4370–4379 (1972).
47. L. Gao, F. Lemarchand, and M. Lequime, "Exploitation of multiple incidences spectrometric measurements for thin film reverse engineering," Opt. Express **20**(14), 15734–15751 (2012).
48. J. Kim, A. Dutta, G. V. Naik, A. J. Giles, F. J. Bezares, C. T. Ellis, J. G. Tischler, A. M. Mahmoud, H. Caglayan, O. J. Glembocki, A. V. Kildishev, J. D. Caldwell, A. Boltasseva, and N. Engheta, "Role of epsilon-near-zero substrates in the optical response of plasmonic antennas," Optica **3**(3), 339–346 (2016).
49. N. Kinsey, C. DeVault, J. Kim, M. Ferrera, V. M. Shalaev, and A. Boltasseva, "Epsilon-near-zero Al-doped ZnO for ultrafast switching at telecom wavelengths," Optica **2**(7), 616–622 (2015).
50. J. Rydén, B. Hjörvarsson, T. Ericsson, E. Karlsson, A. Krozer, and B. Kasemo, "Unusual kinetics of hydride formation in Mg-Pd sandwiches, studied by hydrogen profiling and quartz crystal microbalance measurements," J. Less-Common Met. **152**(2), 295–309 (1989).
51. J. E. Schirber and B. Morosin, "Lattice constants of β-PdHx and β-PdDx with x near 1.0," Phys. Rev. B **12**(1), 117–118 (1975).
52. G. V. Naik, J. Kim, and A. Boltasseva, "Oxides and nitrides as alternative plasmonic materials in the optical range [Invited]," Opt. Mater. Express **1**(6), 1090–1099 (2011).
53. I. R. Hooper and J. R. Sambles, "Dispersion of surface plasmon polaritons on short-pitch metal gratings," Phys. Rev. B **65**(16), 165432 (2002).
54. J. Zhang, Y. C. Zhou, Z. S. Ma, L. Q. Sun, and P. Peng, "Strain effect on structural and dehydrogenation properties of MgH2 hydride from first-principles calculations," Int. J. Hydrogen Energy **38**(9), 3661–3669 (2013).
55. N. Skryabina, N. Medvedeva, A. Gabov, D. Fruchart, S. Nachev, and P. de Rango, "Impact of Severe Plastic Deformation on the stability of MgH2," J. Alloys Compd. **645**, S14–S17 (2015).